CARBON 52 (2013) 122–127

Available at www.sciencedirect.com

SciVerse ScienceDirect

journal homepage: www.elsevier.com/locate/carbon

Theoretical characterization of reduction dynamics for graphene oxide by alkaline-earth metals

Sheng-Yi Xie [a,d], Xian-Bin Li [a,d,*], Y.Y. Sun [b], Yong-Lai Zhang [a], Dong Han [a,b], W.Q. Tian [a,c], Wen-Quan Wang [d], Yi-Song Zheng [d], S.B. Zhang [a,b,*], Hong-Bo Sun [a,d,*]

[a] State Key Laboratory on Integrated Optoelectronics, College of Electronic Science and Engineering, Jilin University, Changchun 130012, China
[b] Department of Physics, Applied Physics, & Astronomy, Rensselaer Polytechnic Institute, Troy, NY 12180, USA
[c] State Key Laboratory of Theoretical and Computational Chemistry, Institute of Theoretical Chemistry, Jilin University, Changchun 130012, China
[d] College of Physics, Jilin University, Changchun 130012, China

ARTICLE INFO

Article history:
Received 14 July 2012
Accepted 9 September 2012
Available online 17 September 2012

ABSTRACT

First-principles calculation identifies elementary processes in the thermal reduction of graphene oxide (GO) and reveals the effects of alkaline-earth metals (AEMs) in recovering the graphene. These metals are highly effective in removing residual oxygen groups resistive to thermal reduction, as well as healing the defects formed during the reduction, such as the carbonyl groups. In the AEM-assisted reduction, the AEMs serve as an electron reservoir of high chemical potential that forces electron transfer to the GO, whereas pristine carbon regions on the GO serve as a "bridge" to facilitate the electron transfer directly to oxidized carbon. This enables fast kinetics for the breaking of both C–O and C=O bonds. Complete reduction is observed in our simulation at $T \leq 600$ K within 32 ps for a 28%-oxygen-coverage GO model.

1. Introduction

Graphene is a potential candidate material for next-generation electronics [1–3]. However, mass production of graphene under normal experimental conditions remains to be a challenge. Graphene is usually fabricated by mechanical exfoliation [4], by heating silicon carbide to high temperatures (>1100 °C) [5,6], or by epitaxial growth on metal substrates such as ruthenium [7], iridium [8], copper [9], or platinum [10]. Recently, reduction of graphene oxide (GO) has emerged as an important alternative for graphene production, as the method is based on a convenient, high-yield, low-cost solution process. Solution-based GO can be spin-coated on various substrates – a process that is well suited for electronic device fabrications [11].

The reduction of GO typically involves three steps [12]: oxidation of graphite to GO; dispersion of the GO in water; and removal of oxygen groups from the dispersed GO sheets by chemical reduction to form graphene. Several experimental methods have been proposed to reduce GO. High-temperature annealing is simple, clean, and has industrial compatibility with batch processing, but the conductivity is 2 to 3 orders of magnitude smaller than that of pristine graphene [13–16]. Hydrazine reduction can take place at room temperature (RT), which is particularly suitable for plastic substrate. However, hydrazine is toxic and may introduce electrically-active N centers [17]. In this regard, sodium borohydride may be a better choice, as it works at RT without the contamination. However, the conductivity is even lower, about 5 orders of magnitude smaller than that of pristine graphene [18]. In

* *Corresponding authors Address:* State Key Laboratory on Integrated Optoelectronics, College of Electronic Science and Engineering, Jilin University, Changchun 130012, China .
E-mail addresses: lixianbin@jlu.edu.cn (X.-B. Li), zhangs9@rpi.edu (S.B. Zhang), hbsun@jlu.edu.cn (H.-B. Sun).
0008-6223/$ - see front matter
http://dx.doi.org/10.1016/j.carbon.2012.09.012

some sense, hydrogen gas reduction may work better [19], as it is not only clean but can also repair defective aromatic structures. However, potential safety hazard of hydrogen in industrial application is a concern. Meanwhile, HI is found to be another high efficient and quick reducing agent [20–22]. Femtosecond laser ablation, on the other hand, has the ability of region-selective GO reduction, but a too strong and focused energy beam may lead to obvious lattice destroy [23,24]. Only very recently, metals such as Fe [25] and Zn [26] have been used to reduce GO with promising results. However, until now none of these methods can completely reduce GO into graphene. Meanwhile, many defects can also be produced. So, that seriously set a barrier of making high-quality graphene by the ways for actual device application.

Theoretical modeling can provide insights on the structural evolution of the GO to enable better design and comprehension of the reduction process. Classical force-field molecular dynamic study [27] revealed desorption of H_2O from nearby hydroxyls during thermal annealing, and the formation of highly stable carbonyl and ether groups. The latter, however, hinders a complete reduction of the GO to graphene. Annealing in H_2 atmosphere can improve to some degree oxygen removal due to the formation of extra H_2O. Our *ab initio* molecular dynamics (AIMD) simulation, on the other hand, reveals that in thermal reduction, hydroxyls (OHs) desorb from GO in the form of H_2O, as a result of OH diffusion and the formation of nearest-neighbor OH pairs. This desorption is, however, a self-terminating process – as the density of the OH group is reduced, the remaining OH groups prefer to be spatially isolated to maximize the configuration entropy [28], which prevents further desorption. In comparison, epoxies are even harder to desorb. When two epoxies diffuse and become a nearest-neighbor pair, they are more likely to be transformed into a carbonyl pair, which is detrimental to the preparation of defect-free graphene.

In this paper, using AIMD we study the physics that dictates the recovery of graphene from GO. We propose a convenient and potentially highly effective method to completely reduce GO by using calcium or magnesium. The physics of the recovery lies in the charge transfer between the reducing agent (Ca or Mg) and GO ascribed to the difference in the local Fermi level between the two. Charge transfer, however, cannot take place unless there co-exist regions of pristine graphene and those with oxygen groups. The pristine graphene serves as a "bridge" to engage the charge transfer for GO reduction, which takes place only at the boundaries between these two regions. In the presence of Ca, both the C=O and C–O bonds of the oxygen groups can be broken at 600 K. The reaction kinetics is fast – in our simulation, a complete reduction, along with complete removal of carbonyls, has been achieved within several tens picoseconds. It is expected that the reaction products, CaO and $Ca(OH)_2$, can be easily removed by hydrochloric acid [29].

2. Computational details

Our AIMD as implemented in the VASP codes [30] uses a 32-carbon atom graphene unit cell, 1 fs time step, and the canonical *NVT* ensemble, in which the Nosé-Hoover thermostat is used to control the temperature [31]. Γ-point is used in the Brillouin zone sampling. We have tested the results with smaller time step of 0.2 fs, which could be important to hydrogen motion. The results, however, showed no qualitative difference. Experimental thermal reduction temperature ranges from 400 to 1400 K [13,15]. To ensure the observation of GO reduction within a reasonable simulation time, we use a somewhat higher T = 1800 K, but still far below the theoretical melting point of graphene [32].

3. Results and discussion

3.1. *Thermal reduction*

The dynamics of thermal reduction at 1800 K shows characteristic features in terms of (1) the formation and desorption of H_2O and (2) the formation of stable defects as a result of the H_2O desorption. While the atomic structure of GO is currently under intense debate [33–36], it is generally accepted that oxygen exists on GO mainly in the form of epoxy and OH groups [37,38]. Fig. 1 shows the effects of H_2O desorption using an OH-only model [33] with initial oxygen coverage at 38%. Our simulation reveals that OH can readily diffuse on the graphene. Water desorption is initiated when two OHs move together to form a hydrogen bond (between O1 and O2 in Fig. 1(a)). The formation of the hydrogen bond leads to the breaking of the O1 single bond (to graphene substrate) and the lift-up of O1 in Fig. 1(b). The hydrogen bond is subsequently shifted to O2 (see Fig. 1(c)). The shifted hydrogen bond is, however, unstable and the O1-involving H_2O eventually desorbs (see Fig. 1(d)). The O2 left behind is stabilized by forming an epoxy.

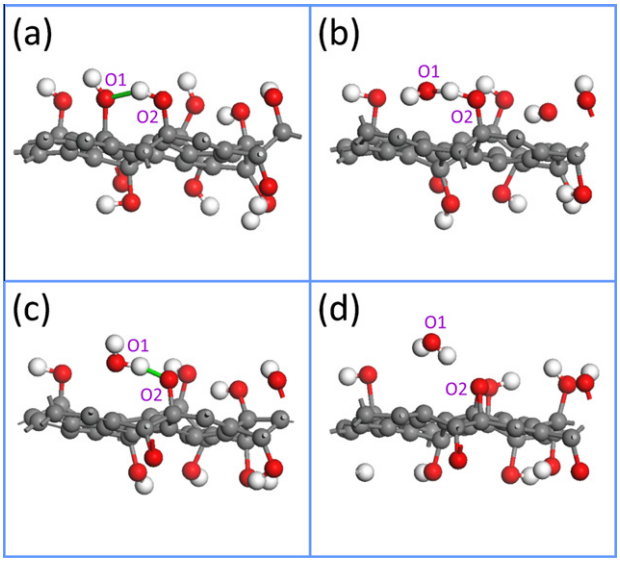

Fig. 1 – MD snapshots (a)–(d) of oxygen desorption in the form of H_2O at 1800 K. Green lines in (a) and (c) indicate the hydrogen bond that has been shifted from O1 in (a) to O2 in (c) through stage (b), resulting in desorption of H_2O in (d). Red balls are O, grey balls are C, and white balls are H. (For interpretation of the references to colour in this figure legend, the reader is referred to the web version of this article.)

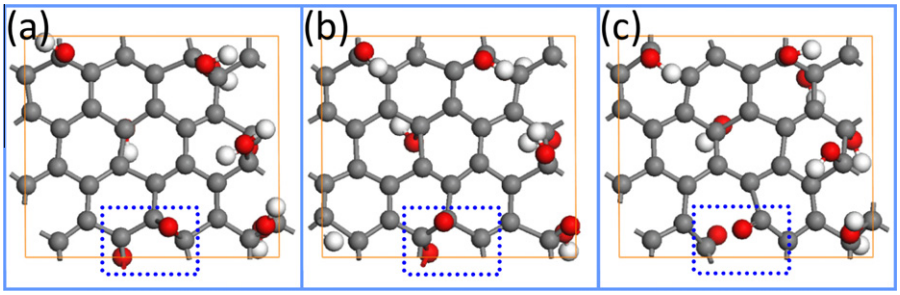

Fig. 2 – MD snapshots showing the formation process of a carbonyl defect on a partially reduced GO surface. Dotted boxes mark the position where a pair of carbonyls forms: (a) an initial epoxy pair, (b) a transition state where the oxygen pair undergoes a lift-up process, and (c) the final carbonyl pair. The legends are the same as in Fig. 1.

Fig 2 shows the effect of thermal reduction on epoxy using a mixed OH and epoxy model, which could also be viewed as the result of aforementioned water desorption. Our simulation reveals that it is difficult to thermally desorb epoxies at 1800 K. Instead, these epoxies are the precursors for the formation of carbonyl (C=O) groups. The epoxies can diffuse on the graphene just like OH. When two epoxies share a C–C bond (see Fig. 2(a)), the bond breaks through an oxygen lift-up process (Fig. 2(b)) followed by a bond rotation process (Fig. 2(c)). Once the rotation is over, two carbonyl groups are created, which not only makes the residual O too stable to be thermally removed, but also leads to the breaking of the underlying graphene network. This is consistent with a recent classical force-field MD study [27].

It appears that both water desorption and carbonyl formation are local processes. Therefore, the results on thermal reduction are relatively insensitive to the details of the structural models used in the simulation.

One may compare the simulation with experiment. The simulation reveals H_2O desorption and carbonyl formation in line with experiment [27,39]. However, neither process reduces the number of C–O bonds; therefore, strictly speaking, no GO reduction has taken place in the simulation, which is at variant with experiment. The only process that can contribute to GO reduction is the epoxy desorption but it has not been observed in the simulation. The reason may be attributed to the short simulation time affordable in the current AIMD. Since in the presence of hydrogen, epoxy may be converted into OH [27], it could thus be beneficial to introduce H either from ambient or intentionally. This enables oxygen removal by the same OH process described in Fig. 1. In the end, a thermally reduced GO (hereof denoted as *thr*-GO) should have sparsely distributed hydroxyl and epoxy groups, as well as certain amount of carbonyl defects.

3.2. *Alkali-earth metal (AEM)-assisted reduction*

Mg, Ca, Sr, and Ba are known for their chemical reducing ability, in accordance with their Pauling electronegativity [40]. In fact, Ca has been widely used for reducing metals from their oxides such as ZrO_2 [41], Sm_2O_3 [42], La_2O_3 [43], and TiO_2 [44]. To assess the effect of the metal on GO, we consider a *thr*-GO with 4 OHs and two carbonyl pairs (one carbonyl stabilizes as a pyran-like form) in a 32-carbon cell, which is resistive to thermal reduction at 1800 K. Before the MD, each side of the *thr*-GO cell is covered by 4 Ca atoms, with a Ca–Ca distance close to that of bulk Ca. It turns out that the detailed structure of the Ca is unimportant, only the density matters.

Fig 3 shows snapshots of the MD simulation. A Ca-graphene distance of 5 Å is used in the initial configuration in Fig. 3(a) (t = 0 ps). Since the starting distance for Ca in real experiment will be significantly longer, the simulated reduction time here will be considerably shorter than what may be realized experimentally. The simulation temperature is 300 K. Fig. 3(b) shows an intermediate MD configuration (t = 4 ps) at which all the hydroxyls have been removed from the *thr*-GO and transferred to Ca. However, reduction of carbonyls has not taken place, due to the significantly larger bond energy of C=O (8.0 eV) versus 1.5 eV for C–OH [45]. Despite the large difference, our simulation reveals that carbonyls can be reduced within a reasonable simulation time at 600 K. Fig. 3(c) shows the final MD configuration (t = 32 ps from the initial configuration or 11 ps after the temperature has been raised from 300 to 600 K) at which the GO is completely reduced. Fig. 3(d)–(f) show the calculated Ca density of states (DOS) corresponding to the three atomic configurations in Fig. 3(a)–(c). Note that, accompanied with the formation of CaO and $Ca(OH)_2$, the system Fermi level (E_F) steadily decreases. The decrease can be attributed to the formation of Ca–O bonding states at significantly lower energies, as indicated by arrows in Fig. 3(e) and (f). Similar results are obtained for Mg.

To understand the underlying mechanism, Fig. 4 shows the DOS and the difference in the E_F's between an isolated Ca layer [E_F(Ca)] and *thr*-GO [E_F(GO)], as it determines the direction of charge transfer. In a real process, Ca must approach GO from distance. To accurately determine the charge transfer direction in this process, we place the Ca and *thr*-GO 9.6 Å apart in the same supercell to minimize their interaction yet to maintain the same energy reference. Fig. 4 shows that E_F(Ca) is higher than E_F(GO) by 0.39 eV. Fig. 4 also decomposes the DOS for carbon atoms to reveal that pristine C has significant amount of *empty* states below E_F(Ca). In contrast, C bonded to oxygen has significantly less empty states below E_F(Ca). Therefore, GO reduction is an electron transfer process from Ca to GO and the transferred electrons are primarily on pristine C.

To generalize the above observation, we calculate several GOs with different OH coverages. Fig. 5(a) shows the position of their empty states, i.e., the conduction band minimum (CBM), relative to E_F(Ca). Insets in Fig. 5 show the correspond-

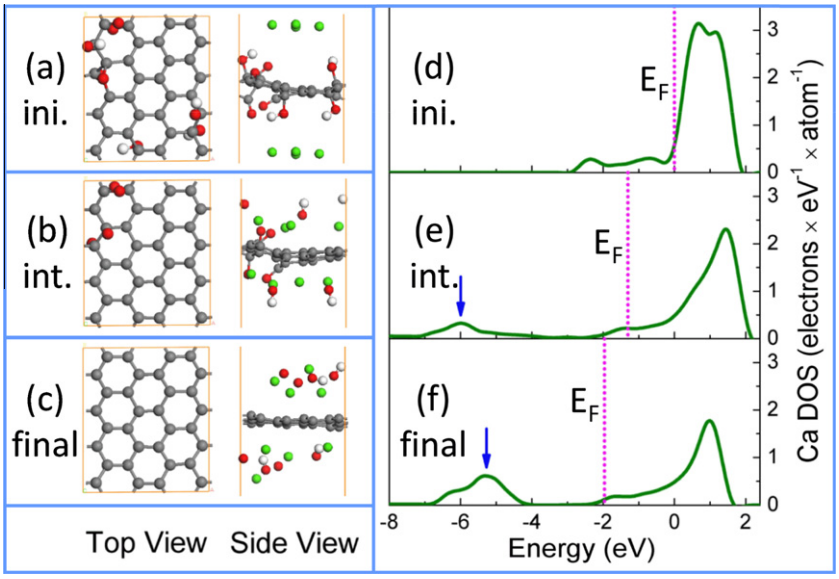

Fig. 3 – Reduction of *thr*-GO in the presence of Ca. We start with *thr*-GO at 300 K, simulate for 20 ps, increase *T* steadily to 600 K in 1 ps, and then simulate for another 11 ps. (a)–(c) (left panel) Snapshots of the initial (t = 0), intermediate (t = 4 ps), and final (t = 32 ps) stages of the reduction along with (d)–(f) (right panel) the respective DOS for Ca. Green balls are Ca. Others are the same as in Fig. 1. Blue arrows indicate Ca bonding states. (For interpretation of the references to colour in this figure legend, the reader is referred to the web version of this article.)

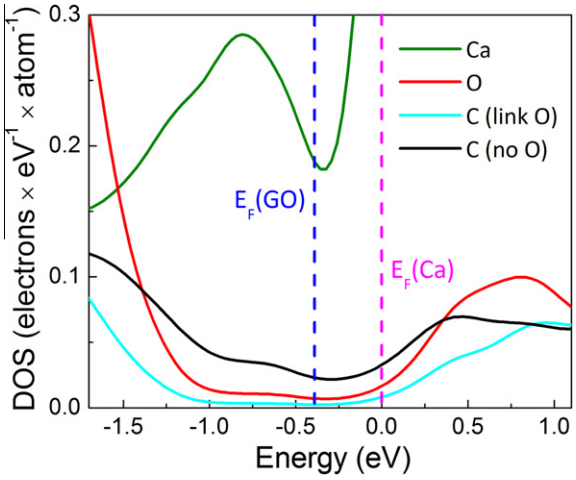

Fig. 4 – Element-selected DOS of an isolated *thr*-GO with 28% oxygen coverage and that of an isolated Ca layer. The DOS for each element is normalized. Carbon has been separated into two subgroups: those with oxygen bonding and those without it. Vertical dashed lines indicate the Fermi level positions of the two isolated systems.

ing spatial charge distribution of the CBM state for 38, 50, and 94% OH coverage, respectively. Indeed, in all cases except for 100% coverage where no charge transfer can take place, electrons from Ca are always transferred to the CBM states around the pristine carbon. This can be understood that the band gap from pristine carbon by quantum confinement effect is generally smaller than that from oxygen-covered carbon by oxygen bonding effect. The first C–O pairs broken in the GO reduction are always located at the interface between the pristine carbon and oxidized carbon. This is understandable, as GO reduction requires the electron injection directly to the oxidized carbon. Fig. 5(b) shows the time required to break the first C-O bond and transfer an OH (at low coverage) or H_2O (at high coverage) to Ca in our MD simulation at 300 K. Not only that water desorption no longer require the formation of OH pair, but also OH can directly be desorbed by the Ca. This is a great benefit of the Ca-assisted reduction over thermal reduction in terms of eliminating the residue oxygen groups.

The above discussion suggests that in an experiment, one should maximize the interfacial regions to increase GO reduction efficiency. When the coverage is high, the interfacial region decreases. Therefore, for coverage of 94%, the time required for GO reduction is significantly longer as shown in Fig. 5(b). When the coverage is 100%, due to the lack of charge transfer, GO reduction is completely stopped. The slightly longer time around 50%, on the other hand, reflects the structural stability of the GO model with that particular oxygen distribution [33].

To experimentally realize Ca reduction of GO, we suggest CaH_2 powder as the Ca source, because CaH_2 can be decomposed into Ca and H_2 at around 1000 K [46] – both are beneficial to GO reduction. Fig. 3(c) shows that, after the reduction, the Ca products – CaO, $Ca(OH)_2$, and un-reacted Ca only weakly interact with fully recovered graphene. The Ca's can all be removed by hydrochloric acid [29],

$$CaO(s) + H_2O(l) = Ca(OH)_2 \quad (1)$$

$$Ca(s) + 2H_2O(l) = Ca(OH)_2(s) + H_2(g) \quad (2)$$

$$Ca(OH)_2(s) + 2HCl(g) = CaCl_2(s) + 2H_2O \quad (3)$$

where the final product $CaCl_2$ is water-soluble and hence can be readily washed away.

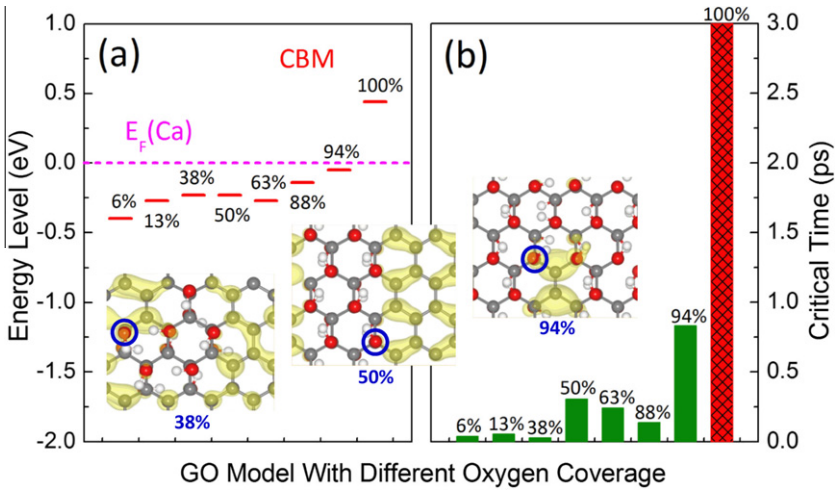

Fig. 5 – (a) CBM (conduction band minimum) of isolated GO at different hydroxyl coverages with respect to E_F of an isolated Ca layer. Insets show charge distribution of the CBM states at 38%, 50%, and 94% coverage, respectively. (b) Critical time required for the breaking of the first C–O bond (circled in the insets) to initiate GO reduction at 300 K. We define the bond breaking as when the C–O distance equals 1.4 times the sum of the corresponding covalent radii. At 100% coverage, no GO reduction takes place. Instead, Ca moves away from GO, indicating that their mutual attraction ceases.

3.3. *Mechanism comparison of the different reduction methods*

All reductions involve electron transfer to oxygen. In thermal reduction or when using the chemicals (like hydrazine, sodium borohydride and hydrogen gas), reactive species such as atomic H [47] must first move to an O atom and then donates its electron by forming a bond directly with the O. As a consequence of random walk during atomic diffusion and its slowness, such a reduction generally requires relatively high temperature and takes hours to get a conductivity of ~1000 S/m [15–18]. In contrast, the AEM mechanism relies on the transfer of itinerate electrons to GO without any prerequisite of atomic diffusion and/or local bonding. Therefore, it is much simpler and faster. It is conceivable that the recent experiments using Fe [25] or Zn [26] for GO reduction may have followed a similar mechanism as that of AEM. The results for Zn are already remarkable: at RT it can reduce the GO within several minutes to reach conductivity as high as 15000 S/m. The reducibility of the metals has the following trend, Ca > Mg > Zn > Fe [40]. This suggests that AEMs could have even better results than either Zn or Fe.

4. Conclusions

AIMD simulations reveal atomic-scale processes for GO thermal reduction. It shows that water desorption has much faster kinetics than that of epoxy. It can also cause the formation of stable carbonyl defects. As such, thermal reduction is ineffective in eliminating residual oxygen groups. On the other hand, alkali-earth metals are highly effective in reducing GO not only because it can accelerate oxygen desorption but also because it can eliminate carbonyl defects to recover perfect graphene lattice. The physical mechanism for alkali-earth metal-assisted GO reduction is identified as the relaying of three charge transfer steps: (a) from Ca to pristine carbon empty states, (b) from pristine carbon to oxidized carbon, and (c) from oxidized carbon to oxygen at the reaction site. Our study offers new insights on how to massive produce high-quality graphene substrates.

Acknowledgements

This work was funded by the NSFC (No. 11104109, 61008014), the TNList Cross-discipline Foundation, and China Postdoctoral Science Foundation (No. 2011M500593). SBZ and YYS acknowledge US DOE Office of Basic Energy Sciences (Grant No. DE-SC0002623) and the National Nuclear Security Administration, Office of Nuclear Nonproliferation Research and Engineering (NA-22). WQT acknowledge Open Project of SKLSSM in JLU (sklssm2012066). We thank the High Performance Computing Center at JLU for computing resources.

REFERENCES

[1] Castro Neto AH, Guinea F, Peres NMR, Novoselov KS, Geim AK. The electronic properties of graphene. Rev Mod Phys 2009;81:109–62.
[2] Geim AK. Graphene: status and prospects. Science 2009;324:1530–4.
[3] Schwierz F. Graphene transistors. Nat Nanotechnol 2010;5:487–96.
[4] Novoselov KS, Geim AK, Morozov SV, Jiang D, Zhang Y, Dubonos SV, et al. Electric field effect in atomically thin carbon films. Science 2004;306:666–9.
[5] Berger C, Song ZM, Li TB, Li XB, Ogbazghi AY, Feng R, et al. Ultrathin epitaxial graphite: 2D electron gas properties and a route toward graphene-based nanoelectronics. J Phys Chem B 2004;108:19912–6.
[6] Emtsev KV, Bostwick A, Horn K, Jobst J, Kellogg GL, Ley L, et al. Towards wafer-size graphene layers by atmospheric pressure graphitization of silicon carbide. Nat Mater 2009;8:203–7.

[7] Sutter PW, Flege JI, Sutter EA. Epitaxial graphene on ruthenium. Nat Mater 2008;7:406–11.
[8] Pletikosić I, Kralj M, Pervan P, Brako R, Coraux J, N'Diaye AT, et al. Dirac cones and minigaps for graphene on Ir(111). Phys Rev Lett 2009;102:056808-1–4.
[9] Li XS, Cai WW, An JB, Kim S, Nah J, Yang DX, et al. Large-area synthesis of high-quality and uniform graphene films on copper foils. Science 2009;324:1312–4.
[10] Gao LB, Ren WC, Xu HL, Jin L, Wang ZX, Ma T, et al. Repeated growth and bubbling transfer of graphene with millimetre-size single-crystal grains using platinum. Nat Commun 2012;3:699–705.
[11] Gilje S, Han S, Wang MS, Wang KL, Kaner RB. A chemical route to graphene for device applications. Nano Lett 2007;7:3394–8.
[12] Dreyer DR, Park S, Bielawski CW, Ruoff RS. The chemistry of graphene oxide. Chem Soc Rev 2010;39:228–40.
[13] Wang X, Zhi LJ, Müllen K. Transparent, conductive graphene electrodes for dye-sensitized solar cells. Nano Lett 2008;8:323–7.
[14] Schniepp HC, Li JL, McAllister MJ, Sai H, Herrera-Alonso M, Adamson DH, et al. Functionalized single graphene sheets derived from splitting graphite oxide. J Phys Chem B 2006;110:8535–9.
[15] Zhou Y, Bao QL, Tang LA, Zhong YL, Loh KP. Hydrothermal dehydration for the "green" reduction of exfoliated graphene oxide to graphene and demonstration of tunable optical limiting properties. Chem Mater 2009;21:2950–6.
[16] Zhu YW, Stoller MD, Cai WW, Velamakanni A, Piner RD, Chen D, et al. Exfoliation of graphite oxide in propylene carbonate and thermal reduction of the resulting graphene oxide platelets. ACS Nano 2010;4:1227–33.
[17] Stankovich S, Dikin DA, Piner RD, Kohlhaas KA, Kleinhammes A, Jia YY, et al. Synthesis of graphene-based nanosheets via chemical reduction of exfoliated graphite oxide. Carbon 2007;45:1558–65.
[18] Shin HJ, Kim KK, Benayad A, Yoon SM, Park HK, Jung IS, et al. Efficient reduction of graphite oxide by sodium borohydride and its effect on electrical conductance. Adv Funct Mater 2009;19:1987–92.
[19] Wu ZS, Ren WC, Gao LB, Liu BL, Jiang CB, Cheng HM. Synthesis of high-quality graphene with a pre-determined number of layers. Carbon 2009;47:493–9.
[20] Pei SF, Zhao JP, Du JH, Ren WC, Cheng HM. Direct reduction of graphene oxide films into highly conductive and flexible graphene films by hydrohalic acids. Carbon 2010;48:4466–74.
[21] Zhao JP, Pei SF, Ren WC, Gao LB, Cheng HM. Efficient preparation of large-area graphene oxide sheets for transparent conductive films. ACS Nano 2010;4:5245–52.
[22] Moon IK, Lee JH, Ruoff RS, Lee HY. Reduced graphene oxide by chemical graphitization. Nat Commun 2010;1:73–8.
[23] Zhang YL, Guo L, Wei S, He YY, Xia H, Chen QD. Direct imprinting of microcircuits on graphene oxides film by femtosecond laser reduction. Nano Today 2010;5:15–20.
[24] Zhang YL, Chen QD, Xia H, Sun HB. Designable 3D nanofabrication by femtosecond laser direct writing. Nano Today 2010;5:435–48.
[25] Fan ZJ, Wang K, Yan J, Wei T, Zhi LJ, Feng J, et al. Facile synthesis of graphene nanosheets via Fe reduction of exfoliated graphite oxide. ACS Nano 2011;5:191–8.
[26] Mei XG, Ouyang JY. Ultrasonication-assisted ultrafast reduction of graphene oxide by zinc powder at room temperature. Carbon 2011;49:5389–97.
[27] Bagri A, Mattevi C, Acik M, Chabal YJ, Chhowalla M, Shenoy VB. Structural evolution during the reduction of chemically derived graphene oxide. Nat Chem 2010;2:581–7.
[28] Chan TL, West D, Zhang SB. Limits on passivating defects in semiconductors: the case of Si edge dislocations. Phys Rev Lett 2011;107:035503-1–4.
[29] House JE. Inorganic chemistry. Oxford: Elsevier; 2008.
[30] Kress G, Furthmüller J. Efficient iterative schemes for ab initio total-energy calculations using a plane-wave basis set. Phys Rev B 1996;54:11169-1–11169-18.
[31] Bylander DM, Kleinman L. Energy fluctuations induced by the Nosé thermostat. Phys Rev B 1992;46:13756-1–6.
[32] Zakharchenko KV, Fasolino A, Los JH, Katsnelson MI. Melting of graphene: from two to one dimension. J Phys: Condens Matter 2011;23:202202–5.
[33] Wang L, Sun YY, Lee K, West D, Chen ZF, Zhao JJ, et al. Stability of graphene oxide phases from first-principles calculations. Phys Rev B 2010;82. 161406-1(R)–161406-4(R).
[34] Yan JA, Xian LD, Chou MY. Structural and electronic properties of oxidized graphene. Phys Rev Lett 2009;103:086802-1–4.
[35] Boukhvalov DW, Katsnelson MI. Modeling of graphite oxide. J Am Chem Soc 2008;130:10697–701.
[36] Lu N, Huang Y, Li HB, Li ZY, Yang JL. First principles nuclear magnetic resonance signatures of graphene oxide. J Chem Phys 2010;133:034502-1–7.
[37] Cai WW, Piner RD, Stadermann FJ, Park SJ, Shaibat MA, Ishii Y, et al. Synthesis and solid-state NMR structural characterization of ^{13}C-labeled graphite oxide. Science 2008;321:1815–7.
[38] Gao W, Alemany LB, Ci LJ, Ajayan PM. New insights into the structure and reduction of graphite oxide. Nat Chem 2009;1:403–8.
[39] Jung I, Field DA, Clark NJ, Zhu YW, Yang DX, Piner RD, et al. Reduction kinetics of graphene oxide determined by electrical transport measurements and temperature programmed desorption. J Phys Chem C 2009;113: 18480–6.
[40] Pauling L. The nature of the chemical bond. IV. The energy of single bonds and the relative electronegativity of atoms. J Am Chem Soc 1932;54:3570–82.
[41] Abdelkader AM, El-Kashif E. Calciothermic reduction of zirconium oxide in molten $CaCl_2$. ISIJ Int 2007;47: 25–31.
[42] Jones FG, Tokunaga M. Low temperature coefficient cobalt-rare earth magnets. IEEE Trans Magn 1976;12: 968–70.
[43] Ohtsuka M, Kim DY, Itagaki K. Formation of RE_xNi_y (RE = La, Ce, Pr or Nd) compounds by calciothermic reduction of La_2O_3, CeO_2, Pr_6O_{11} and Nd_2O_3. J Alloys Compd 1995;230:46–52.
[44] Chen GZ, Fray DJ, Farthing TW. Direct electrochemical reduction of titanium dioxide to titanium in molten calcium chloride. Nature 2000;407:361–4.
[45] Acik M, Lee G, Mattevi C, Chhowalla M, Cho K, Chabal YJ. Unusual infrared-absorption mechanism in thermally reduced graphene oxide. Nat Mater 2010;9:840–5.
[46] Hu JJ, Xiong ZT, Wu GT, Chen P, Murata K, Sakata K. Hydrogen releasing reaction between $Mg(NH_2)_2$ and CaH_2. J Power Sources 2006;159:116–9.
[47] Kim MC, Hwang GS, Ruoff RS. Epoxide reduction with hydrazine on graphene: a first principles study. J Chem Phys 2009;131:064704-1–5.